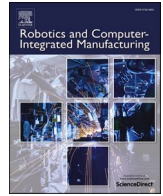




Contents lists available at ScienceDirect

# Robotics and Computer-Integrated Manufacturing

journal homepage: [www.elsevier.com/locate/rcim](http://www.elsevier.com/locate/rcim)

## Seam tracking and gap bridging during robotic laser beam welding via grayscale imaging and wobbling

Davide Maria Boldrin<sup>a</sup>, Lorenzo Molinari Tosatti<sup>b</sup>, Barbara Previtali<sup>a</sup>, Ali Gökhan Demir<sup>a,\*</sup><sup>a</sup> Department of Mechanical Engineering, Politecnico di Milano, Via La Masa 1, 20156 Milan, Italy<sup>b</sup> National Research Council of Italy, Via A. Corti 12, 20133 Milan, Italy

## ARTICLE INFO

## Keywords:

Laser welding  
Closed-loop control  
Wobbling  
Robotic welding

## ABSTRACT

The use of laser beam welding with robotic manipulators is expanding towards wider industrial applications as the system availability increases with reduced capital costs. Conventionally, laser welding requires high positioning and coupling accuracy. Due to the variability in the part geometry and positioning, as well as the thermal deformation that may occur during the process, joint position and fit-up are not always acceptable nor predictable *a-priori* if simple fixtures are used. This makes the passage from virtual CAD/CAM environment to real production site not trivial, limiting applications where short part preparations are a need like small-batch productions. Solutions that render the laser welding operations feasible for production series with non-stringent tolerances are required to serve a wider range of industrial applications. Such solutions should be able to track the seam as well as tolerating variable gaps formed between the parts to be joined. In this work, an online correction for robot trajectory based on a grayscale coaxial vision system with external illumination and an adaptive wobbling strategy are proposed as means to increase the overall flexibility of a manufacturing plant. The underlying vision algorithm and control architectures are presented; the robustness of the system to poor illumination conditions and variable reflection conditions is also discussed. The developed solution employed two control loops: the first is able to change the robot pose to follow varying trajectories; the second, able to vary the amplitude of circular wobbling as a function of the gap formed in butt-joint welds. Demonstrator cases on butt-joint welds with AISI 301 stainless steel with increased complexity were used to test the efficacy of the solution. The system was successfully tested on 2 mm thick, planar stainless-steel sheets at a maximum welding speed of 25 mm/s and yielded a maximum positioning and yaw-orientation errors of respectively 0.325 mm and 4.5°. Continuous welds could be achieved with up to 1 mm gaps and variable seam position with the developed control method. The acceptable weld quality could be maintained up to 0.6 mm gap in the employed autogenous welding configuration.

### 1. Introduction

Laser welding has been adopted by the industry in various applications for delivering high quality welds with high penetration, low heat input and relatively high speeds. Anthropomorphic robots are dexterous manipulators that can perform complex trajectories with smooth motions, highly adaptable for complex part geometries. A combination of the two should allow for high manufacturing flexibility, small to medium batch products with geometrical variations. On the contrary, the mainstream of robotic laser welding is often limited to simpler weld geometries and standardized part geometries [1] or more focused to arc welding. Laser welding requires tight tolerances and stringent

conditions for relative positioning of the laser tool and parts [2]. As a matter of fact, laser welding often requires the previous manufacturing steps to have better tolerances to avoid gaps and misalignments before and during welding [3]. Moreover, rigid and dedicated fixtures are often needed to ensure gap elimination [4,5]. Such conditions are highly disadvantageous for small to medium sized lots and complex geometries. The correct positioning between the parts and the laser beam puts the emphasis on the path accuracy of the manipulator. In this regard, robots generally display good repeatability but low accuracy [6], especially when required to follow complex trajectories that involve tool reorientations [7]. The two issues cause the translation from CAD/CAM virtual environment to the physical welded parts to be often not

\* Corresponding author.

E-mail address: [aligokhan.demir@polimi.it](mailto:aligokhan.demir@polimi.it) (A.G. Demir).<https://doi.org/10.1016/j.rcim.2024.102774>

Received 24 November 2023; Received in revised form 1 March 2024; Accepted 1 April 2024

0736-5845/© 2024 The Author(s). Published by Elsevier Ltd. This is an open access article under the CC BY-NC-ND license (<http://creativecommons.org/licenses/by-nc-nd/4.0/>).

satisfactory without external intervention. From this perspective, seam tracking devices and process solutions to weld in the presence of gap formation are essential.

Correction techniques to absorb the mismatches between nominal and real trajectories are not new topics to literature and industry [8,9]. Above all, seam-tracking allows for reduced downtimes, by introducing live corrections to the laser trajectory while the weld is being performed. With laser welding, seam-tracking is to meet stringent positioning requirements, as the maximum allowable error is in the range of the spot dimension, i.e. even as small as 0.2 mm [2,10]; in this regard, more traditional joining technologies like arc welding and deriving have a clear advantage. The literature shows that excellent results are possible with robotic arms on simple weld geometries: the robot's tool center point (TCP) could be made to track linear welding trajectories on planar sheets with accuracies better than 0.3 mm [11–17] and as good as 0.15 mm in [18–20]. Performances diminish instead if a robotic arm is required to also reorient the laser head while tracking. This is unavoidable when following seams along curved surfaces; it is also the case of curved weld paths on planar surfaces if the laser head is equipped with auxiliaries that require a certain angle (usually yaw angle) with respect to the abscissa, e.g. wire or gas nozzles. De Graaf et al. demonstrated [10] robot seam-tracking accuracy values varying from 0.1 mm for a straight butt joint to 0.5 mm for a sine-shaped butt joint revolving on a curved surface. An accuracy of 0.7 mm was shown by Jia et al. on a saddle-shaped weld trajectory [21]. These results are in full agreement with the tests and simulations on industrial robot arms discussed by Waiober [7]. If orientation can be fixed, path accuracy is also improved, as shown in [22], where a maximum error of 0.2 mm was obtained on curved trajectories. Different strategies have been proposed to save the robot yaw reorientations on planar welds such a redundant in-hand degree of freedom [23] to adjust the angle of wire nozzle and yields a 0.3 mm accuracy along curved welds on planar sheets. Iakovou et al. [24] developed a perimetric sensor for remote autogenous laser welding, which surrounds the TCP of the robot with a triangle of uninterrupted sensing. An alternative is to use the robotic arm to follow a nominal trajectory and let more accurate, higher-dynamics positioners deal with the inaccuracies of the real weld trajectory. Using such strategy a system featuring galvanometric scanners on a remote weld head is shown to produce an outstanding 0.1 mm accuracy in [25]. This approach though can very finely guide the laser spot, it does not center all other auxiliaries that have a fixed position with respect to the weld head and this, above all, hampers the use of shielding gas and filler wire [26]. Multiple authors proposed the combination of a robotic arm and a linear stage mounted on the robot flange (the so-called “micro-macro” robot layout) to solve this problem [18,27,28]. The former follows the nominal trajectory, while the latter superimposes its corrections and slides the whole laser head in cross-direction. This approach can give good results but is generally bulkier and limited to correct along one direction only. In general, linear stages allow for more accurate positioning of the laser as shown by Cieszynski et al. [29] on a dedicated machine for circular welds and by Shao et al. [30] on a more general-purpose, 7-axis cartesian robot. The main disadvantage of such systems remains the cost limiting their industrial use. Finally, path accuracy can be improved by seam-mapping, i.e. by dry-running the robot with the sensing system on the joint before welding is started. Seam mapping was applied by Yan et al. [31] and a maximum error of 0.36 mm could be obtained on a planar, curved trajectory involving yaw-angle reorientation. An iterative seam-mapping approach for repetitive weld parts was also proposed in [27]. Dry-runs entail longer setup times and iterative approaches can yield a significant quantity of failed parts. It emerges that the state-of-the-art accuracy of seam-trackers during laser welding along curved trajectories is only adequate for laser welding with wide spots [10]. Recent advancements in robotic welding seam tracking emphasize the integration of advanced vision systems [32–35], machine learning algorithms [33,34], and multi-sensor approaches [36–39] to enhance accuracy, adaptability, and automation in welding processes. The latest

research effort has been chiefly focused on arc welding applications, suggesting that the main limits for the applicability to a quality joining technique like laser welding lies in the higher positioning accuracy it requires. It appears therefore important to further explore methods for relaxing the laser welding precision requirements. With the reduction cost of automation and laser systems along with the development of new data analysis methods the need for seam tracking devices have gain relevance in the recent years.

Another issue regarding the precision requirements of laser welding regards the gap formation. Adaptive wobbling can be seen as a way to reduce the sensitivity of the laser to positioning accuracy and at the same time cope with gap formation during the laser welding operations. By wobbling, the width of the laser-material interaction zone can be expanded without the need to use a wider beam and while also maintaining the high irradiance of the small spot [40–45]. Rubben et al. showed the welding of 1.2 mm-thick sheets with gaps up to 0.3 mm and 0.8 mm vertical mismatch by means of wobbling [46]. Vanska et al. used wobbling for longitudinal welding of tubes improving gap bridgeability on austenitic 4 mm and 5 mm thick stainless steel tubes [47]. Köhler et al. [48] showed gaps up to 0.4 mm on 2 mm thick 1.7131 steel butt joints could be achieved with wobbling. The use of wobbling for gap bridging on other joint configurations, thicknesses, and materials have been shown confirming the suitability of such solution for fixed and known gap formation conditions [49–53]. On the other hand, the use of an external sensor to adapt the wobbling strategy, especially its amplitude, has not been previously demonstrated. Moreover, the combination of a seam-tracker for laser welding with beam wobbling is an open challenge with great potential for a greater use of robotic welding technology in the industry. A combination of the complimentary advantages of the two control approaches has not been treated in the literature and it is not implemented in turnkey commercial products to the authors' knowledge.

Accordingly, this work proposes two online control systems for improving the flexibility of robotic welding systems in the presence of positioning errors and gap formation. The two systems consist of i) a seam-tracker based on a coaxial vision-guided motion control architecture for robot pose control, and ii) a wobble amplitude control for gap bridging based on a feed-forward architecture employing the same coaxial vision architecture. The solutions were developed for welding 2 mm thick AISI 301LN stainless steel sheets in butt joint configuration with welding speeds below 50 mm/s. A curved planar profile was tracked with a maximum error of 0.325 mm, enough for a continuous weld thanks to the use of dynamic beam-shaping. This also allowed the bridging of a gap as wide with a sound weld up to 0.5 mm.

## 2. System development

### 2.1. Robotic laser welding cell

The tests were carried out on a flexible robotic welding system (BLM Adige, Levico Terme, Italy). The system was equipped with a 6 kW fiber laser source (IPG Photonics YLS 6000) employing a 100  $\mu\text{m}$  delivery fiber and a beam parameter product (BPP) of 3.3 mm-mrad. The laser was coupled to a wobbler head (IPG Photonics D50). The head featured a camera mount for coaxial monitoring, a 300 mm focal and 200 mm collimation lens. The resulting theoretical Rayleigh length was 1.5 mm, while the focused beam diameter was 150  $\mu\text{m}$ . An anthropomorphic robot with 6 degrees of freedom (ABB IRB4600) held the laser head while a tilting-rotary table (ABB IRBPA250) could manipulate the workpiece. An image of the laser cell is reported in Fig. 1a, while Fig. 1b shows the detail of the laser head with ancillary systems.

### 2.2. Coaxial grayscale vision system

At the basis of the two control systems described in this article lies a custom coaxial active imaging apparatus. Images were taken by a

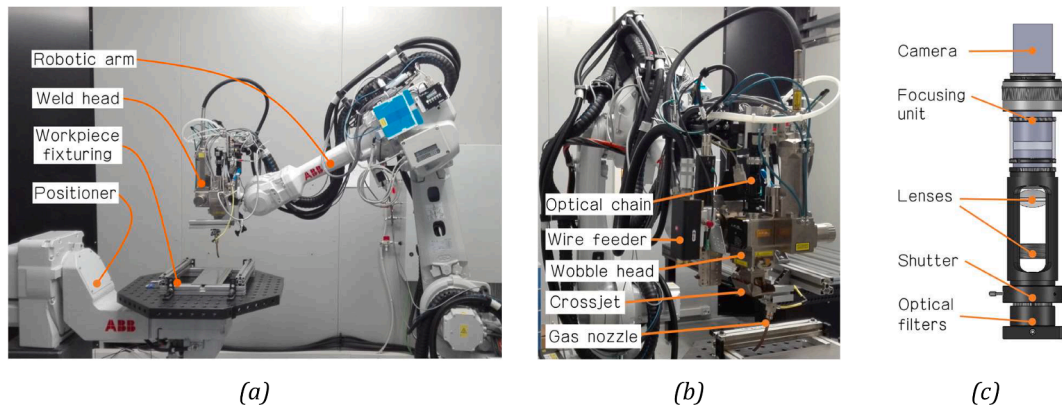


Fig. 1. The developed robotic laser beam welding cell and weld control system: a) the robotic cell, b) the wobble head, c) the optical chain.

monochromatic camera (Ximea CMOS, XiC MC031MG) with pixel size of  $3.45 \mu\text{m}$  and resolution of  $2064 \times 1544$ . An LED illuminator by (Advanced Illumination, SL164) with a wavelength of  $660 \text{ nm}$  was used to illuminate the weld area and produce grayscale images. A custom optical chain is coupled to the camera to fulfill some key requirements for the imaging system:

- Optical resolution of  $20 \mu\text{m}/\text{px}$ , to distinguish small features such as ideal  $0 \text{ mm}$  gap butt joints, that have a typical dimension of  $0.1 \text{ mm}$  [30].
- Depth of field of  $15 \text{ mm}$ , to obtain focused images from the coaxial camera even when laser is defocused (up to  $\pm 5 \text{ mm}$ ) for technological purposes.
- Field of view of  $8 \text{ mm} \times 5 \text{ mm}$ , to image the seam and a significant part of the surrounding region.
- Optical filtering to obtain clear images of the seam during welding.

The resulting optical chain used two camera lenses to fulfill requirements on resolution and depth of field. An iris was also present to regulate camera aperture, critical for the depth of field. A  $660 \text{ nm}$  band-pass filter was used to selectively let illumination light through and reject process noise. The choice of such a wavelength came from spectrometric measurements of process emission during welding of most common materials and joint configurations. An additional  $750 \text{ nm}$  low-pass filter further cuts off NIR emission and laser back-reflection. The CAD model of the optical chain can be seen in Fig. 1c.

### 3. Development of the seam tracking and gap control strategies

Two control systems are proposed in this article for increased process adaptability. A seam-tracker addresses the issue of robot path accuracy by adjusting the robot tool central point (TCP) over the seam as well as the orientation of the laser head. The second control system, instead, acts on the wobbling amplitude to adapt it to the gap width and enhance the gap-bridging capability.

#### 3.1. The control approach

Despite the optical filters employed, a significant quantity of noise is received from the weld pool. To reduce its effects on seam detection the region of interest (ROI) of the vision algorithm was placed away from the laser spot, further along the seam at a fixed look-ahead distance, called *forerun*. This means that a certain interval exists between the moment a portion of the seam is sensed in the look-ahead ROI and the moment it is hovered over by the trailing robot TCP. In fact, the correction actions entailed in image  $k$ , taken at time  $t_k$ , are not due before time  $t_k + \Delta t$ , where such delay can be approximated as:

$$\Delta t = \frac{fr}{v_w} \quad (1)$$

where  $fr$  is the forerun and  $v_w$  is the welding speed. This additionally means that, after a starting wind-up period equal to  $\Delta t$  in which the forerun is filled with seam detection, at any time the references of real seam pose and gap width will be known in advance. On the one hand, this is beneficial for smooth planning of corrections [28] and allows to compensate for possible delays in the actuators. On the other hand, anything happening to the seam after the moment it was sensed is unobservable. Hence, too long a forerun should be avoided [10]. In the work of Regaard et al. [28], typical forerun values are indicated to lay between  $40 \text{ mm} - 200 \text{ mm}$ . In this work, forerun was set to  $6 \text{ mm}$ , minimizing the issues on observability but at the same time requiring higher robustness to the noise coming from the close weld pool.

#### 3.2. Grayscale online vision algorithm

The proposed image analysis algorithm was based on active grayscale vision. An off-axis, diffused LED source illuminates the workpiece surface, and a coaxial camera obtains images of the scene. The variable scattering of light on the surface provides the 2D information of its features. Amongst such features, seam center position, seam orientation, and gap width were extracted and used for control purposes. The camera was operated with an automatic exposure control. Exposure time is adjusted for each frame to have a  $50 \%$  average brightness in the area close to the seam to counteract possible variations in surface reflection. The seam extraction process itself was based on both gradient and region-based methods and consists of the 5 steps shown in Fig. 2.

1. ROI and preprocessing: A ROI is set to image the seam  $6 \text{ mm}$  away from the laser tool (forerun). The  $x$  axis of camera  $x^{(c)}$  is always almost parallel to seam direction as a result of robot control (Fig. 2a) so a fixed ROI can be used with width  $100 \text{ px}$  (along  $x^{(c)}$ ) and height  $400 \text{ px}$  (along  $y^{(c)}$ ), respectively corresponding to  $1.8 \text{ mm}$  and  $7.2 \text{ mm}$ . A wider ROI could have been applied for a better spatial knowledge of the seam and its surrounding context; given the small forerun and the presence of a resulting very high process noise, a smaller ROI was selected to allow for higher frequencies in image acquisition and analysis ( $100 \text{ Hz}$ ), this way yielding a faster monitoring of the seam at the cost of a narrower context analysis. The ROI was blurred with a Gaussian filter with kernel  $3 \times 3$  as a precaution against the high-frequency noise that can sometimes originate from small-pixel-size sensors operated with little amount of light and fast exposures.
2. Directional gradient: To make the desired features stand out, the blurred image is processed with a Sobel kernel to obtain the  $2^{\text{nd}}$  degree gradient along  $y^{(c)}$  axis. A monodirectional kernel is chosen to

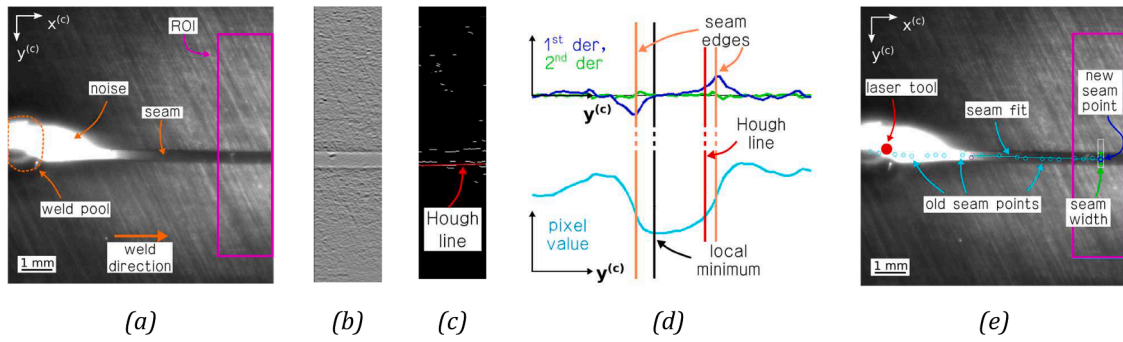


Fig. 2. The implemented real-time greyscale algorithm: a) original image, b) gradient image, c) Hough image, d) seam width estimate, e) seam fit and recognition.

reduce disturbance from secondary edges. The principal edges that belong to the seam are always almost aligned with  $x^{(c)}$  axis. Kernel size is  $5 \times 5$ , this way providing an additional blurring along  $x^{(c)}$  direction to further alleviate noise issues. Gradient image is visible in Fig. 2b.

- Edge extraction: To extract the most relevant features, the gradient image is fed to a self-adjusting Canny algorithm [54,55] run with variable thresholds for edge enucleation and growth. These are first set according to the histogram of the gradient image (respectively selecting 95<sup>th</sup> and 90<sup>th</sup> percentile) and subsequently adjusted by a feed-back loop. Aim of such an approach is to keep the number of lines recognized in each image to a desired quantity, this way complying with the varying illumination conditions.
- Line extraction: Despite the previous filtering steps, the edge image still contains some secondary edges. To isolate the seam edges, Hough transform [56] is employed and only those lines are extracted that are at least 40 px long (i.e. 40 % of ROI width), located close to the expected position of the seam edge, and have an angle close to the expected seam angle (Fig. 2c). The expected seam position and angle are determined by linear fitting of the 10 previous points. Linear fitting was chosen for its higher speed with respect to higher dimensional fits as it can still be applied to curved trajectories without significant drawbacks. In fact, given the high framerate (100 fps) and low speeds (25 mm/s - 50 mm/s), the linear approximation can hold also for significantly curved trajectories. Two seam edge lines would be expected in each image. In cases when the small, unavoidable unevenness in the utilized metal sheet causes a high enough vertical step between the two sides of the butt-joint, the directional light could draw a shade on the lower side, this way obscuring one edge and making the other stand out more clearly for recognition. This phenomenon occurred frequently, in approximately half of the images for the selected material and joint configuration. For a more stable seam detection, a final region-based search step is therefore added, as explained in the following point. Finally, in extreme cases when no edge could be detected at all, the prediction of its location by linear fit was utilized.
- Width estimate: To estimate width, the distance between the two seam edge lines could be used. Since these were not always both available, another method was preferred. A cross-section of the blurred ROI (Fig. 2a) along the vertical  $y^{(c)}$  axis was taken around the point of detected/fitted seam edge from step 4. The values of these pixels are shown as the light-blue curve in the lower half of Fig. 2d; the  $y^{(c)}$  coordinate of the Hough line detected in the previous step is instead drawn as a vertical red line. The light-blue curve is then searched for the local minimum that is closest to the Hough line (black vertical line in Fig. 2d). This represents the darkest point in the joint and the borders of the seam can be found as the closest two critical points in the first derivative of the curve (shown as the dark-blue curve in upper half of Fig. 2d). Such critical points must lay within a certain distance from the minimum. Seam center is

estimated as the average point between these two extrema and seam width as their distance projected along the direction perpendicular to seam edges. A linear fit of the previous 10 valid gap width estimates is used for comparison to the new estimate. If the estimation is too distant, it is rejected and fitted value is used instead.

The combination of step 4 and 5 was observed to give the best results with varying illumination conditions. The darkest points in the ROI are not always located in the seam and this can lead to wrong identifications. Picking the global minimum of the light-blue line in Fig. 3 would result in an erroneous detection. It was worthwhile to provide a more robust initial guess in the form of Hough line(s), which turned out to be less sensitive to variable illumination: this allowed to shrink the search span of step 5 and reduce the risks of picking up undesired shadow areas. Finally, seam pose was taken as the center of the gap and the angle of the seam fit line was used to estimate the seam yaw.

The described algorithm was then applied in different imaging conditions. Thanks to the self-adjustment concept, the localized search for seam and filtering of outliers, the detection could be carried out stably even in the presence of non-ideal conditions such as bright specular reflections, low-light and process noise, as presented in Fig. 4.

### 3.3. Robot trajectory adjustment

This control loop is responsible for controlling the robot TCP over the seam in cases of unforeseen modifications to the nominal welding trajectory. At the base of robot control is a proprietary package by ABB, the Externally Guided Motion Position Guidance (hereafter referred to simply as EGM) [57,58]. Based on a UDP socket, it outputs the current robot pose and expects the next setpoint to move to, both with a frequency 250 Hz. This way, one can only specify a stream of positions for the robot to reach but cannot influence the loops that grant convergence to them (feedback loops on motor position, speed). For this reason, visual-servoing was not considered as a possible control architecture [6]. Instead, a position-based vision-guided control [59] was utilized, as shown in Fig. 5. The vision algorithm determines the position of the seam center, which represents the target for the robot's external control. The actual robot pose received via EGM is used to calculate the positioning error. A regulator calculates the corresponding control action, which is sent as an operational-space pose to the robot via EGM. Finally, the actual control on joint servos is closed internally to the robot controller and not accessible on the outside. EGM was preferred to the wobble-head scanners for tracking the joint because it allows for an accurate and continuous centering on the seam not only of the laser beam but also of the welding auxiliary systems such as shielding-gas nozzle and filler-wire.

EGM entails a lag between the moment a new setpoint is received by the controller and the moment when the robot starts moving towards it [57,58]. To estimate this value, the robot was commanded to move in space along sinusoidal trajectories and the imposed and actual trajectories were compared to estimate their lags via cross-correlation. The



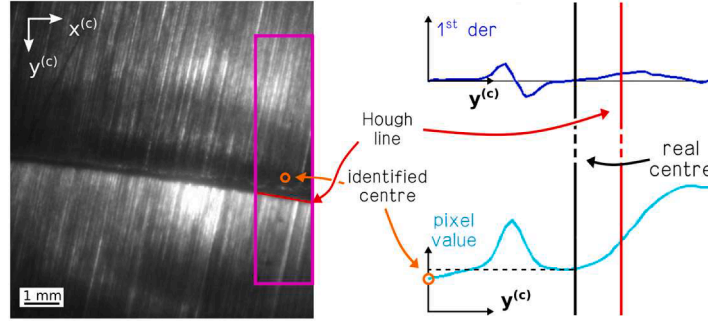


Fig. 3. Error occurrence when skipping Hough step. The darkest point (orange circle) is not within the seam gap.

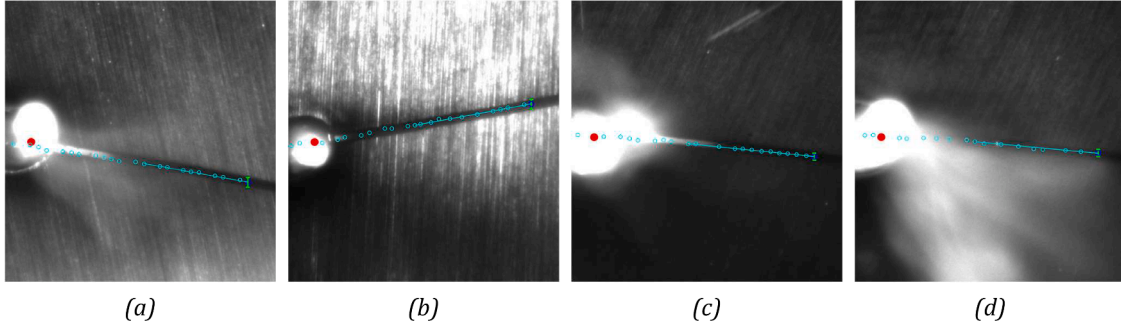


Fig. 4. Different images from seam-recognition algorithm: a) ideal; b) bright reflection; c) low-light; d) process noise.

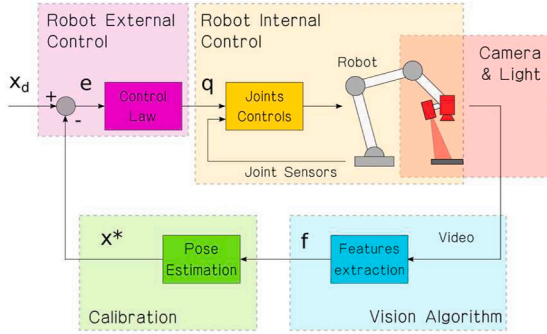


Fig. 5. The devised vision-guided, position-based motion control for seam-tracking.

imposed trajectories had a fixed amplitude of 0.5 mm and different frequencies, up to 6 Hz. This approach yielded a variable value for lag,  $\Delta t_{EGM}$ , ranging from 30 ms to 83 ms stabilizing at higher frequencies as shown in Fig. 6. For the following tests, a value of 60 ms was assumed for  $\Delta t_{EGM}$ . No other significant lag was measured in the imaging nor in the image-analysis and robot-control code, as a result of the lean C++ implementation of software and the choice of a reduced ROI for the camera. In any case, the presence of a forerun allowed for compensation of deterministic delays.

### 3.3.1. Seam position buffering and correction synchronization

The designed system features a 6 mm forerun for reducing process emission disturbance and accounting for robot delays. When welding at 25 mm/s, this corresponds to a  $\Delta t \approx 240$  ms (Eq. (1)) between sensing of the seam and actuation of the corresponding correction for the robot TCP. To assure a timed application of such correction the proposed vision guided control performs three passages: 1) synchronization of robot and camera; 2) buffering of the absolute seam pose estimates; 3) generation of TCP correction via interpolation.

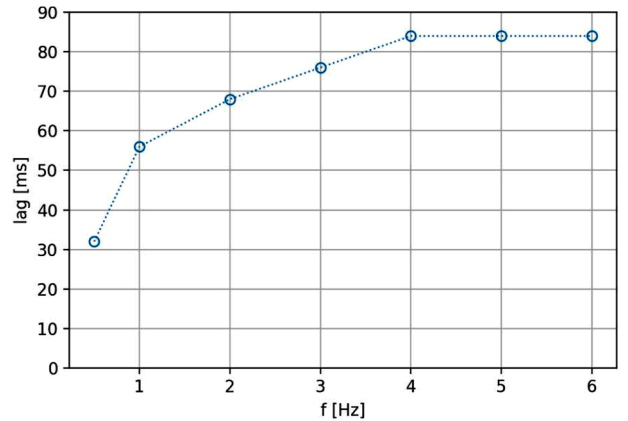


Fig. 6. Lag in the response of EGM to imposed 0.5-mm wide sinusoids as a function of their frequency.

Firstly, synchronization is needed since camera and robot refer to two different clocks. Every image comes with a timestamp that is defined by the camera internal FPGA, while robot poses are instead referred to the PC internal clock. The two independent clocks are therefore synchronized at the beginning of program execution so that such events can be referred to a common time origin. Secondly, since robot poses and camera images are not recorded synchronously (camera frame rate is 100 Hz, EGM frequency is 250 Hz). Hence the reconstruction of the robot position at the time instant  $t_k$  when image  $k$  was taken was done with linear interpolation. The poses of the robot TCP in the base RS  ${}^b_tT$  (subscript “t” stands for TCP and apex “b” for the fixed robot-base RS) that were recorded right before and after  $t_k$  (respectively  ${}^b_tT_j$  at  $t_j$  and  ${}^b_tT_{j+1}$  at  $t_{j+1}$ ) are linearly combined to give  ${}^b_tT_{k,int}$  as shown in Fig. 7.a and with the following expressions:

$${}^b_tT_{k,int} = \alpha {}^b_tT_j + (1 - \alpha) {}^b_tT_{j+1}, \text{ let} \quad (2)$$

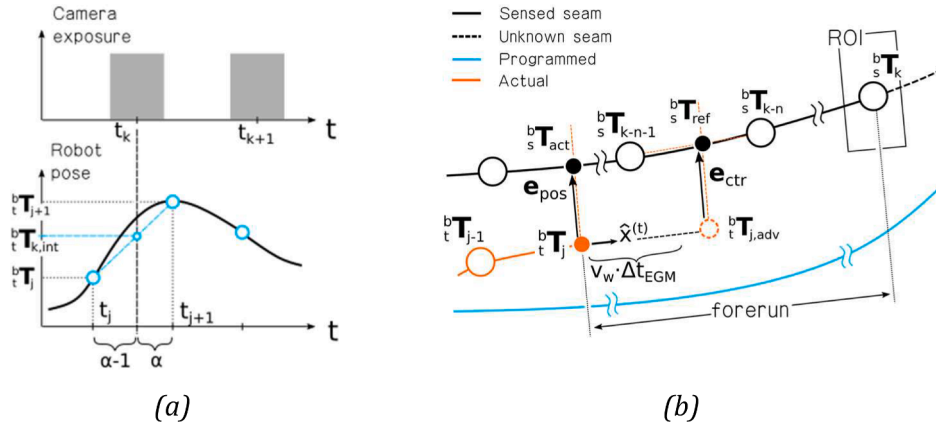


Fig. 7. Two-step interpolation for generation of robot reference pose, a) recording of the poses, b) sensed, actual, and programmed, trajectories.

$$\alpha = \frac{(t_{j+1} - t_k)}{(t_{j+1} - t_j)} \quad (3)$$

Linear interpolation was chosen for its lower computational costs and the small error it induced given the high frequency of robot communication. Having reconstructed the TCP position, by knowing the seam position in camera RS and the position of the camera in the TCP's RS, the seam-center position in base RS  ${}^b_s T_s$  can be found, where "s" subscript stands for seam. Such an estimate is anyway located further ahead by a distance equal to the forerun, so it is stored in a buffer for later use. The seam buffer is re-sampled at every EGM cycle to determine the actual reference for the TCP. The current TCP pose  ${}^b_t T_j$  is read and the two seam buffer entries that are closest to it should theoretically be interpolated, similarly to what is done in Eqs. (2) and 3. EGM entails a systematic delay between receiving a correction and applying it. To prevent this delay from causing inaccuracies or instabilities, corrections are sent ahead of time for compensation. Instead of the two seam entries that are closest to the current TCP position  ${}^b_t T_j$ , the interpolation happens between the two that are closest to the predicted position for the TCP in  $\Delta t_{EGM}$ , namely  ${}^b_t T_{j,adv}$ . These two closest poses from the buffer,  ${}^b_s T_{k-n-1}$  and  ${}^b_s T_{k-n}$ , are linearly combined to generate the reference pose  ${}^b_s T_{ref}$ . The whole procedure is depicted in Fig. 7.b, where three different trajectories are shown. The light-blue lines depict the programmed weld trajectory, corresponding the *a-priori* knowledge of the workpiece geometry. The orange lines show the actual TCP trajectory given by EGM feedback, which is known only at discrete points shown as orange dots. The black lines represent the sensed seam, that is only known up to the forerun and also only at those sections analyzed by the algorithm, shown as black dots. After these steps, seam reference is available as  ${}^b_s T_{ref}$  and control error  $e_{ctr}$  is evaluated as its distance from the advanced TCP pose  ${}^b_t T_{j,adv}$ .

### 3.3.2. Motion regulation

The control error  $e_{ctr}$  was utilized by the seam-tracker for a decentralized robot pose control. The controlled robot degree of freedom (DOF), expressed in the TCP RS (hence the  ${}^{(t)}$  apex), are the abscissa/advancement direction  $x^{(t)}$ , the perpendicular correction along  $y^{(t)}$  axis and the angular correction along the yaw angle  $\psi$  that revolves around  $z^{(t)}$  axis (see Fig. 8). A set of 2 independent PI regulators was utilized for the two corrected DOF, whereas  $x^{(t)}$  coordinate was used for keeping the desired welding speed. Weld trajectories were obtained on planar metal sheets and the utilized grayscale imaging system was used to estimate seam position and orientation on such a plane, whereas perpendicularity and distance from the workpiece surface were enforced *a priori*. As shown in Fig. 8 feed motion is aligned with tool  $x^{(t)}$  axis, lateral correction follows tool  $y^{(t)}$  axis and the yaw angle,  $\psi$ , revolves around  $z$

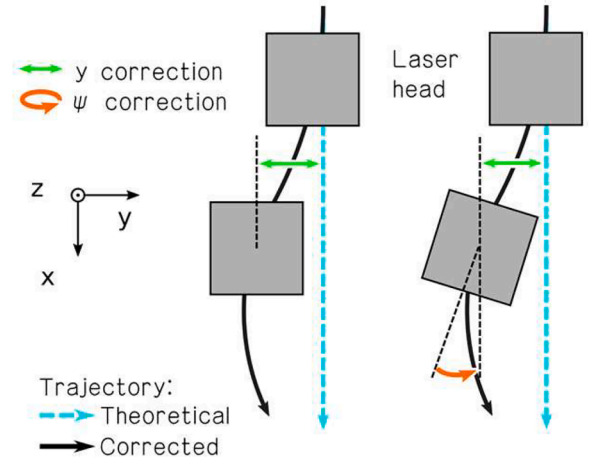


Fig. 8. The controlled DOFs are  $y^{(t)}$  translation and  $\psi$  rotation;  $x^{(t)}$  is the fixed-rate advancement.

axis. The correction of  $y$  accounts for lateral misalignment of TCP with respect to the seam and is the correction applied by most industrial seam-trackers working along planar weld paths. Yaw angle  $\psi$  represents the angle of the weld head around its optical axis and is rarely controlled in scientific literature and industrial practice. It is nonetheless crucial in the case of curved trajectories to maintain a more consistent positioning of gas and wire nozzles.

PI regulators were selected for the convenient control over rise time and steady-state error they offer at a reduced computation cost. No filtering was applied to their input signals. The PI controllers were implemented with anti-windup as custom C++ code. The tuning of PI regulators proved to be a challenging procedure also due to the partial transparency of EGM that only allows for setpoint determination but no action over the internal robot controls. The quasi-deterministic lag  $\Delta t_{EGM}$  generates a destabilizing action on the system. The seam-center estimates output by the vision algorithm entails a low level of noise in the range  $\pm 60 \mu\text{m}$  at a frequency of 100 Hz. The trajectory interpolation steps performed at 250 Hz may also contribute to lowered stability. The tuning problem was therefore tackled with a series of trial-and-error tests on curved trajectories, in an attempt to contain vibrations caused by said uncertainties and noise sources, while also providing a quick enough rise time.

The PI regulators provide the feedback control action, which is then added to the next nominal trajectory point and finally sent to the EGM. The EDM executes the correction after the time interval  $\Delta t_{EGM}$ . A block diagram of the system is shown in Fig. 9.

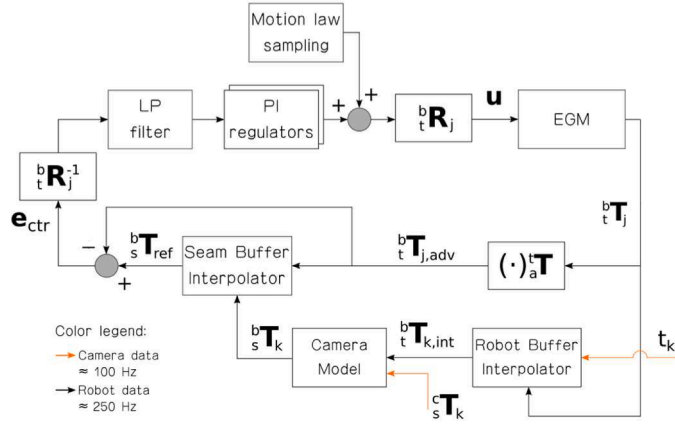


Fig. 9. Seam-tracker architecture with buffering and correction delaying.

### 3.4. Active gap bridging by wobble control

The second control system manages the wobbling amplitude to increase gap-bridging capabilities of the laser welding cell. It is structured as an open-loop control over wobbling parameters (amplitude and frequency) during circular wobbling. The wobble head accepts two analogue signals (0 V - 10 V) to proportionally modulate the wobbling amplitude (from 0 mm to 3 mm) and frequency (from 0 Hz to 700 Hz). A control board (STMicroelectronics, STM32L152RE) was utilized to produce the required signals.

#### 3.4.1. Gap bridging of AISI 301LN sheets by wobbling

To test the gap-bridging capability of laser beam wobbling technique, an experimental campaign was performed to build the control law for wobble parameters in the form of a look up table (LUT). The selected material for the campaign was a 2-mm thick AISI 301LN sheet prepared for butt joint welding. The varied parameters were wobble frequency  $f$ , wobble amplitude  $A$  and gap width  $g$ . The wobble geometry was always circular. Linear tracks of length approximately 200 mm were obtained at constant laser power and speed, respectively 2000 W and 25 mm/s. The investigated levels for gap width, wobble frequency and amplitude are shown in Table 1, together with the other fixed parameters. To obtain the desired gap width in weld tests, calibrated spacers were inserted in between workpieces before the clamping. The maximum dimension of the gap for this test was set to 0.5 mm as an expectable value in the practice of small-batch production.

The quality of the resulting welds was evaluated by analysis of their cross-sections. Samples were cut 20 mm before weld end to expose the steady-state bead properties and mounted. The mounted samples were polished and etched with a solution of distilled water, hydrochloric acid and nitric acid (proportions 1:1:1). Images of the etched samples were

Table 1  
Fixed and varied parameters in the presented gap-bridging campaign.

Fixed parameters	Symbol	Unit	Value
Material	–	–	AISI 301LN
Thickness	$t$	mm	2
Joint type	–	–	Butt-joint
Laser power	$P$	kW	2.0
Defocus	$d_f$	mm	–4
Laser spot	$d_{spot}$	$\mu\text{m}$	430
Wobble geometry	–	–	Circular
Welding speed	$v_w$	mm/s	25
Varied parameters	Symbol	Unit	Value
Gap width	$g$	mm	0 – 0.3 – 0.5
Wobble frequency	$f$	Hz	25 – 50 – 75
Wobble amplitude	$A$	mm	0.5 – 1.0 – 1.5

taken with a Mitutoyo QV202-PRO5F. The lack of filling at head section ( $t_h$ ) and the concavity at the root ( $t_r$ ) were subsequently measured with ImageJ. The measurements were finally classified according to the three levels of quality specified by norm ISO 6520-1:2007 [60] that are reported in Table 2. For a 2 mm thick sheet, the thresholds for stringent, intermediate, and moderate quality are respectively 0.2 mm, 0.4 mm, and 0.6 mm for both investigated parameters. An example of such measurements is reported in Fig. 10. Only samples with a continuous bead were analyzed this way; samples that, instead, displayed discontinuous bridging were discarded and will be reported as 'failed' in the following.

The results of the experimental campaign categorized according to the levels of Table 2 are shown in Fig. 11a. The 0 mm gap condition displays a broad process stability over the tested wobble parameters. By increasing gap width, the process becomes less tolerant up to gap width of 0.5 mm where only one good combination could be found. This condition might represent a manufacturing limit for laser beam welding without filler-wire. In general, the process feasibility range is reduced for higher gap width, and higher wobbling amplitudes are needed as a larger apparent spot size has a better capability of melting and joining the two edges across the gap. Moreover, it was observed that a combination of low frequency and amplitude causes two subsequent wobble circles to not overlap sufficiently on one another. This happens when the overlap between two wobble circles, calculated as  $O = 1 - \frac{v_w}{fA}$  is lower than approximately 0 %. In such cases, the weld edges become jagged and if a gap is present the weld continuity is lost. On the contrary, the combination of high frequency (75 Hz) and amplitude (1.5 mm) implies higher tangential speed for the pool. An increase in material loss with spatter production might be a factor in the failure of such combinations in 0.3 mm and 0.5 mm gap width cases. In the feasibility map conditions indicate the continuity of the weld seam. On the other hand, the increase of the wobbling amplitude in the absence of gaps generates wider seams and increases the spatter generation. Hence, it is more suitable to employ the minimum amplitude conditions that allow gap bridging.

Considering all the requirements the most suitable frequency was found to be at 50 Hz for all gaps. Wobble amplitude was instead varied with gap width to follow the blue dashed line of Fig. 11.a. Fig. 11.b shows the implemented control law.

#### 3.4.2. Control architecture

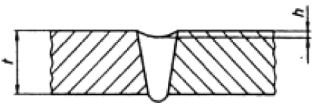
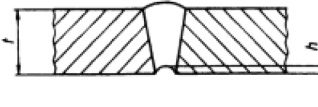
The start point for gap-bridging control is the vision algorithm that provides an estimate of the gap width. As for seam-tracker, the presence of a forerun requires an intermediate layer of buffering and delay. Every seam width estimate is attached to the corresponding seam point so that the same re-sampling of the buffer can be performed. In the case of gap-bridging, though, there is no significant delay in actuation as the galvanometric scanner in the wobble head has fast dynamics and low latency. For this reason, the interpolation step is performed on the two gap width buffer entries whose corresponding seam poses are actually closest to the current TCP pose. Given the estimate of gap width, the corresponding set points for wobble parameters are determined from the LUT of Fig. 11.b. These setpoint values are then passed on to the microcontroller, turned into proportional analogue signals and fed to the wobble controller that produces the final desired amplitude  $A$  and frequency  $f$ . The schematic of the open-loop is visible in Fig. 12.

## 4. Online seam tracking and gap control demonstrator cases

To evaluate the effectiveness of the devised control systems, three tests were performed with an incremental approach, as shown in Fig. 13.

- I) In the first one, the seam-tracker was used to follow a 0 mm gap, butt joint on a planar sheet. The joint geometry was curved while the taught weld trajectory was a straight line so that the control should impose both lateral displacements and yaw angle changes

**Table 2**  
The two analyzed weld imperfections with quality level, according to ISO 6520-1:2007 [60].

Defect	Sketch	Quality level		
		Moderate D	Intermediate C	Stringent B
Incompletely filled groove		$h \leq 0.3 t$ or 1 mm, whichever is the smaller	$h \leq 0.2 t$ or 0.5 mm, whichever is the smaller	$h \leq 0.1 t$ or 0.5 mm, whichever is the smaller
Root concavity		$h \leq 0.3 t$ or 1 mm, whichever is the smaller	$h \leq 0.2 t$ or 0.5 mm, whichever is the smaller	$h \leq 0.1 t$ or 0.5 mm, whichever is the smaller

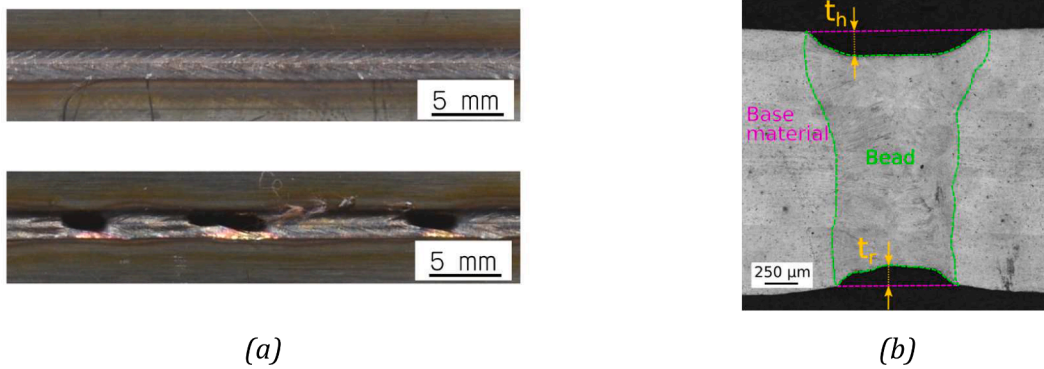


**Fig. 10.** Resulting weld quality: a) weld soundness from surface inspection: continuous above and discontinuous below; cross-sections were evaluated only for continuous welds; b) example of the measurements performed on cross-sections: the depth of head and root concavities, respectively  $t_h$  and  $t_r$ .

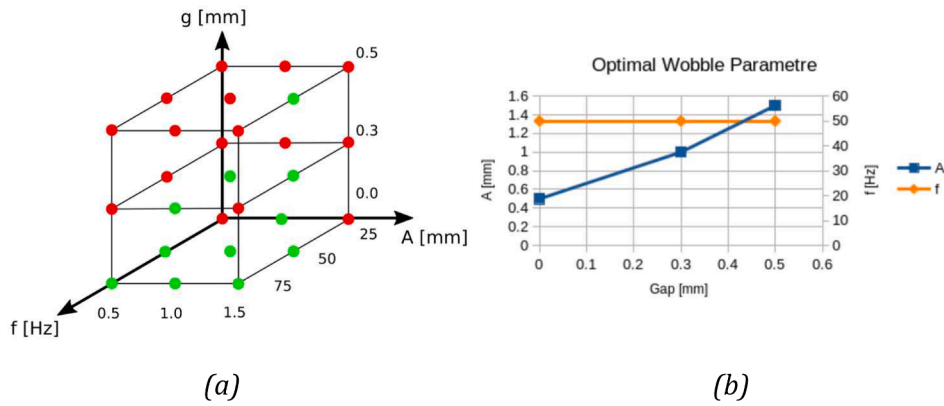


**Fig. 11.** Gap-bridging campaign results: a) gap-bridging capability as evaluated from metallographic cross-sections; b) the resulting control law for wobble parameters.

to keep the right position and alignment with the weld. The test is schematized in Fig. 13a.

- II) The second test instead involved the gap-bridging control alone. A linear butt joint was prepared with a variable gap, ranging from 0 mm to 1 mm and the control adjusted wobbling amplitude to produce a sound weld. The gap variation was wider than 0.5 mm gap which was bridged with sufficient quality. The gap-bridging control test is schematized in Fig. 13b.
- III) In the third test the two control systems were used simultaneously to cope with a curved butt joint with a gap varying from 0 mm to 1 mm as shown in Fig. 13c.

All tests were performed with the same fixed process parameters of Table 1. The wobble amplitude was set to 0.5 mm for the first test for plain seam-tracking. In the other two tests, it was controlled according

to the LUT of Fig. 11.b. In all cases, wobbling geometry was circular.

#### 4.1. Trajectory control via seam tracking

The seam tracking was tested with the curved path and shown as a black solid line in Fig. 14.a, a planar trajectory with a curvature radius of 150 mm. This curvature corresponds to a variation in yaw angle in the range  $\pm 30^\circ$  with a rate of  $10^\circ/\text{sec}$ , both values considered to be challenging for the control system. An AISI 301LN 2-mm thick sheet was laser cut to create edges with such geometry. The edges were then juxtaposed with no gap spacers and workpieces were blocked with the fixtures visible in Fig. 14.c. The robot was instructed to follow a nominal welding path on a straight line along  $x^{(b)}$  axis, drawn as a dashed light-blue line in Fig. 14.a. A trapezoidal velocity motion law was adopted on such path, with a stroke of 300 mm, a trapezoid coefficient  $\xi_v = 0.1$  and



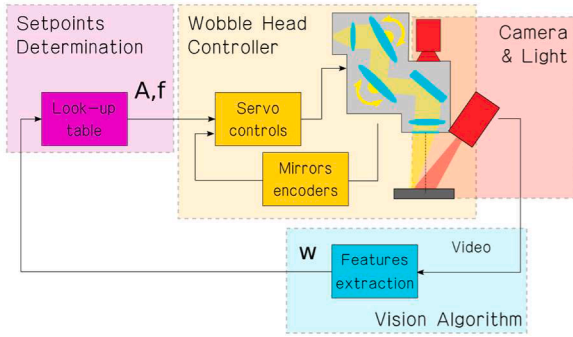


Fig. 12. The control chart of the wobble system employing circular wobbling strategy.

maximum speed equal to 25 mm/s. Such law was chosen to guarantee reduced accelerations ( $a_{max} = 18.8 \text{ mm/s}^2$ ) and have a sufficiently long section of constant speed for welding (approximately 280 mm) as seen in Fig. 14.b.

This zero-prior approach was not chosen as representative of production practice, where offline programming is normally used for the creation of a tighter nominal path. The idea behind it was rather to stress the control system and test it to more demanding conditions in terms of trajectory corrections. A better nominal path could have been used but was not for this reason. To evaluate the overall efficacy of the seam-tracker, the positioning error  $e_{pos}$  was estimated as the distance between the current TCP pose and the closest point re-sampled from the seam buffer. Hence the reconstruction of the seam was used for the error estimate rather than the nominal path. The closest point was found again by linear interpolation of the seam buffer, similarly as what was

described for  $e_{ctr}$ . In the case of  $e_{pos}$  the actual TCP pose was used as a query point and not the advanced one (see Fig. 14.b for reference). Using  $e_{pos}$  as error metrics implicitly assume a perfect match between the real seam geometry and its representation stored in the seam buffer. To fulfil this assumption and accurate seam detection by the algorithm as well as good calibration and synchronization the hardware should be verified.

To test the seam detection algorithm accuracy, the seam poses detected by the algorithm on 100 different frames were compared with the same measurements performed manually by a human operator. The difference between the two is reported as an estimate of algorithm error  $e_{alg}$  in Fig. 15.a. The maximum error was contained under 3 px with a standard deviation of 1.22 px and a mean value of 0.22 px. Considering that sub-pixel seam detection was not implemented, the results appear to be satisfactorily accurate.

To the hardware calibration and synronization, an estimate of the error arising in the generation of absolute seam poses and in the resampling of seam reference ( $e_{ref}$ ) was performed. The nominal joint geometry was compared to that reconstructed by the seam-tracker, evaluated as the locus of all reference points  ${}^b_s T_{ref}$ . This test was performed on the curved joint described earlier and is reported in Fig. 13.b. In order for the two geometries to be comparable, the CAD was registered on the real geometry with a planar roto-translation, as shown in Fig. 15.b. The parameters of such transformation were determined by minimizing the RMS error between the two curves, with a resulting maximum error of 0.1 mm. The comparison to the nominal CAD geometry implicitly assumes perfect tolerances in the manufacturing of parts, which could anyway be held true thanks to the precision of the adopted laser cutting process. Given the good agreement between nominal and measured joint geometry, the assumption of small reference error was considered fulfilled. For these reasons, in the following tests, the performances of the seam-tracker were quantified with the

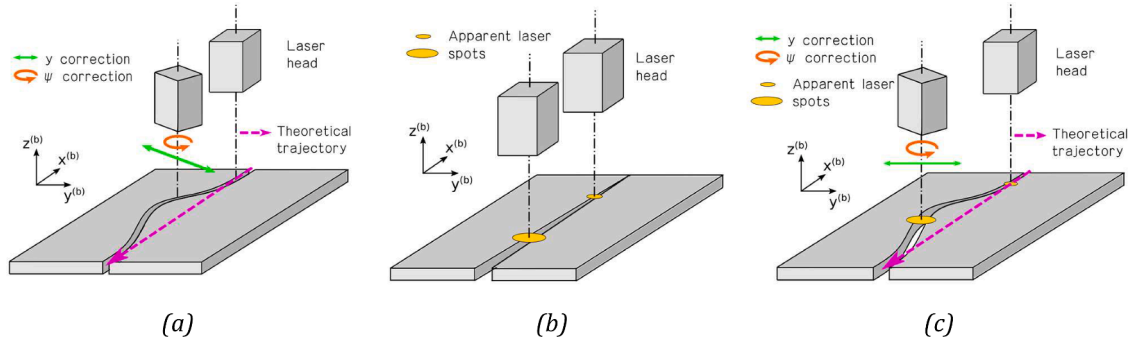


Fig. 13. Schematic description of the tests to evaluate the performance of the seam tracking and gap bridging control. a) Seam-tracking test with a curved track and 0 mm gap. b) Gap-bridging test with linear track and variable gap from 0 mm to 1 mm. c) Seam-tracking and gap-bridging with variable gap from 0 mm to 1 mm.

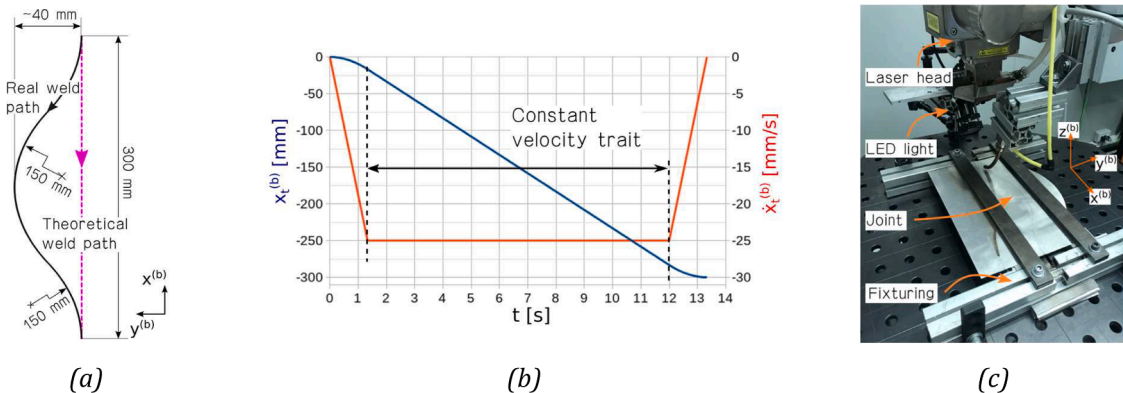


Fig. 14. The details of the seam-tracking test. a) The tested curved welding path, b) the trapezoidal-velocity motion law, and c) the fixtures and setup of the welding tests.

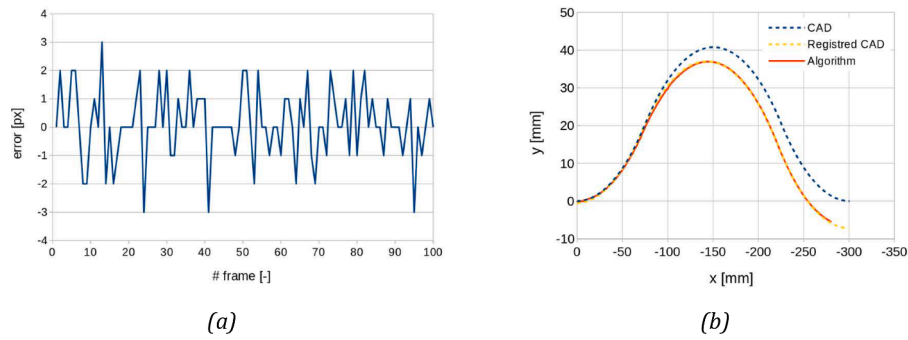


Fig. 15. Estimate of errors in the generation of seam references. a) Algorithm error  $e_{alg}$ , and b) reference error  $e_{ref}$ .

positioning error metrics  $e_{pos}$ .

The results of the seam tracking test are shown in Fig. 16.a as the full trajectory of TCP  $y$  coordinate and yaw angle in robot base RS, respectively  $y_t^{(b)}$  and  $\psi_t^{(b)}$ . The positioning error  $e_{pos}$  for the same two components is shown in Fig. 16.b. The two-time series start after the first acceleration section of the trajectory as the seam-tracker was limited to act only during the constant-speed section ( $t = 1$  s). At the very beginning of the constant-speed section, a high  $y$  error is caused by the off-centered starting position of the robot with respect to the seam but is anyway absorbed very quickly by the control. The highest oscillations in both error signals concentrate around trajectory midpoint ( $t = 7$  s) and are probably related to an imperfect estimate of  $\Delta t_{EGM}$ . A low-frequency component is also observable, anti-symmetric drift with respect to the center of the trajectory curve; this suggests a too low correction action so that higher gains could benefit performances. In any case, the maximum error remains always below 0.4 mm, an advancement with respect to state-of-the-art value for seam-tracking along curved trajectories of 0.5 mm obtained in [10]. Yaw angle error is also kept below  $\pm 6^\circ$ , where the relatively looser control also reflects the higher tolerance in the alignment of wire and gas nozzles to the seam (see Fig. 16.b). The resulting weld is sound, also thanks to the mitigating effect of the 0.5 mm amplitude wobbling (see Fig. 16.c).

#### 4.2. Gap bridging via control of wobble parameters

The gap bridging test was performed on a linear butt joint obtained on the same base material. The gap width was linearly varied from 0 mm to 1 mm along a total track length of 150 mm. The path for the robot was taught manually by operator and the same motion law of the seam-tracking test was utilized (Fig. 14.b). For values of gap width higher than the maximum tested width (0.5 mm), the control wobble amplitude was extrapolated with a linear fit. The wobbling geometry was circular. To evaluate the accuracy of seam width, estimated by the vision algorithm, the joint was also measured manually every 20 mm with a calibrated USB portable optical microscope before welding.

The results of the gap-bridging test are shown in Fig. 17. Fig. 17.a compares the time histories of gap width as measured by the algorithm during welding and with measured values. The two estimates show good

agreement, with a maximum error of 94  $\mu\text{m}$ , a mean error of 3.5  $\mu\text{m}$  and a standard deviation of 22  $\mu\text{m}$ . The welded part is shown in Fig. 17.b. Thanks to the control, the gap is continuously bridged up to 1-mm wide gap. The quality of such weld is anyway only acceptable up to 0.6 mm gap width, as observed in the experimental campaign. Beyond such levels, filler wire would help fill the gap.

#### 4.3. Combined trajectory and wobble control

The same weld geometry of Fig. 14.a was utilized with a butt joint prepared with a linearly increasing gap, from 0 mm to 1 mm. The robot was instructed to follow a nominal linear path along  $x^{(b)}$ . The results of test are shown in Fig. 18. The control error  $e_{ctr}$  shown in Fig. 18.a depicts a low-frequency carrier overlapped to a higher frequency component. Thanks to the tuning of the PI regulators, the maximum  $y$  error was relatively low at approximately 0.325 mm. With respect to the performances of the first test the yaw error was also reduced to  $4^\circ$ . In spite of wide gap variation (see Fig. 18.b), the final weld is continuous to the end of the workpiece. The satisfactory weld quality could be achieved up to 0.6 mm gap, while with wider gaps the seam becomes extremely sagged requiring filler wire (Fig. 18.c). Nonetheless, given the satisfactory seam-tracking result and the bridgeability up to 0.6 mm of gap width, the test is considered successful. The effectiveness of the method can also be further assessed on other gap and position variations that may occur asynchronously and in increasing or decreasing conditions, which will be assessed in future works.

#### 4.4. Observed system limitations

Overall, the results confirm that the employed method was successful in its execution as seen in the trajectory but also successful in maintaining the weld continuity. The employed method can successfully adapt both the robot pose and the wobble amplitude to maintain the gap bridging throughout the process. While the results show a complete framework of system development, the developed strategy remains with application limited to the employed material, thickness, and joint type. From this perspective, the work also provides insights into the open research questions for widening the application of seam tracking beyond

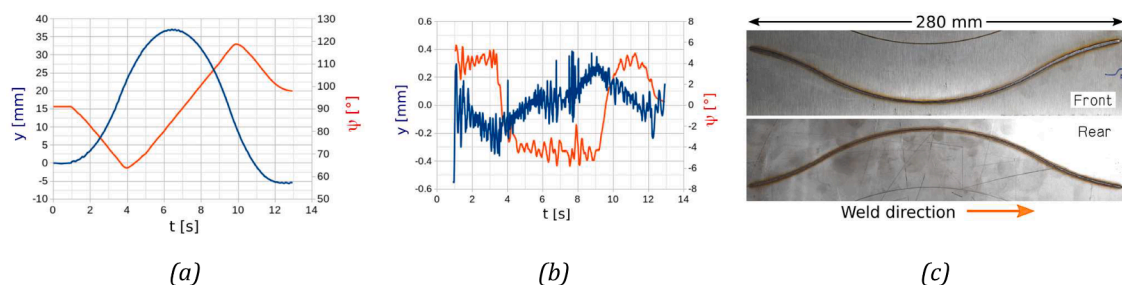


Fig. 16. Results of welding with seam tracking control. a) Corrected trajectories, b) seam-tracker errors  $e_{pos}$ , and c) macro images of the weld seam.

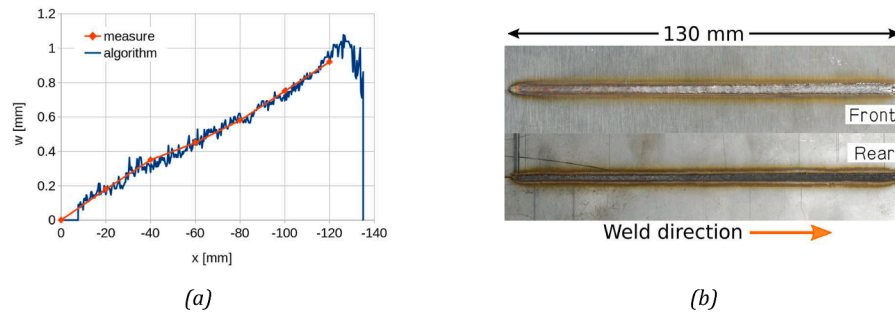


Fig. 17. Results of gap bridging test. a) Gap width time history and b) part welded with wobble parameter control.

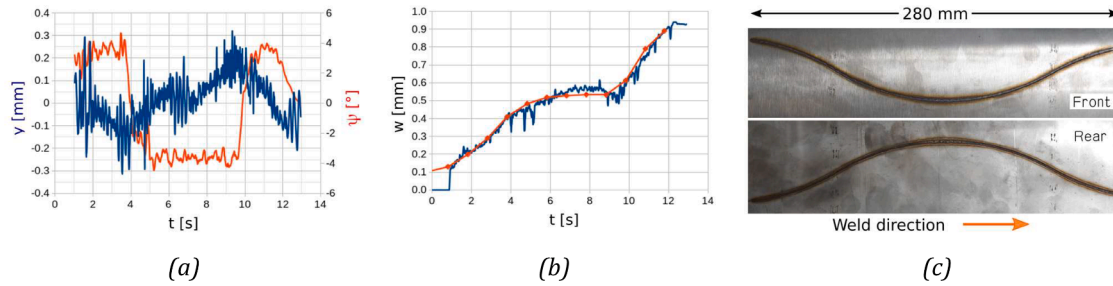


Fig. 18. Results of the combined seam tracking-gap bridging test. a) Seam-tracker errors  $e_{pos}$ . b) Seam width profile where algorithm estimate is shown in blue and the manual measurement in red. c) Macro images of the welded part.

the tested material and thickness combination.

Concerning the seam recognition, the surface texture of the welded material has an important role on the identification of the seam. The tested conditions were more favourable as surface texture due to the rolling direction was not fully parallel to the seam in any of the cases. The algorithm requires further attention towards the robustness against different surface textures or surface imperfections, which were not studied in this work. Similarly, the material type constitutes a source variation in terms of surface reflectivity. Future works will investigate hardware and image processing solutions to overcome these issues. Added to this complexity, the laser welding process parameters should be adapted to the new material types and thicknesses. The use of analytical and numerical models may facilitate to develop the process parameters and validate their use with the monitoring system in an integrated manner.

Throughout the work the gap bridging was achieved without any filler wire. Indeed, the use of filler material is expected to improve the weld quality as well as the extent of gap bridging towards the size of the filler wire above 1 mm. The presence of the wire in the welding zone poses another challenge also from the image analysis perspective. Tilted wire feeding or imaging sensors can be envisaged as aids to improve the system capability.

## 5. Conclusions

The paper describes a control architecture for increasing manufacturing flexibility in robotic laser beam welding of AISI 301LN butt joints via simultaneous seam-tracking and gap-bridging. A custom grayscale vision algorithm for the detection of seam position, orientation and gap is described. The seam-tracker can correct the robot position and orientation on an unknown, curved weld path; the resulting position and orientation errors are respectively below 0.3 mm and 4.5° and the obtained weld is sound. A gap-bridging control is also implemented and tested successfully on a butt joint up to 0.6 mm. The combination of the two systems is therefore proved as a valid solution for absorbing manufacturing inaccuracies and expanding the laser beam welding process window. Given the potentialities of the system, future

efforts will focus on the integration of a second structured-light source for detection of axial distance and 3D geometry. With the added feature it is aimed to maintain the focal position and the laser head position correctly with respect to the surface to maintain the process in control. Such control strategy should indeed require further investigations regarding the sensitivity of the welding operation to the focal position variations as a function of the tested material and joint configuration.

## CRediT authorship contribution statement

**Davide Maria Boldrin:** Conceptualization, Methodology, Formal analysis, Investigation, Data curation, Software, Writing – original draft, Writing – review & editing. **Lorenzo Molinari Tosatti:** Methodology, Supervision, Resources, Writing – review & editing. **Barbara Previtali:** Methodology, Supervision, Resources, Writing – original draft, Writing – review & editing. **Ali Gökhan Demir:** Conceptualization, Methodology, Supervision, Formal analysis, Investigation, Writing – original draft, Writing – review & editing.

## Declaration of competing interest

The authors declare that they have no known competing financial interests or personal relationships that could have appeared to influence the work reported in this paper.

## Data Availability

Data will be made available on request.

## Acknowledgement

The authors gratefully acknowledge the support and the long-standing collaboration of BLM Adige.



## References

- [1] M. Fridenfolk, G. Bolmsjö, Design and validation of a universal 6D seam tracking system in robotic welding based on laser scanning, *Ind. Robot* 30 (5) (2003) 437–448, <https://doi.org/10.1108/01439910310492202>.
- [2] J.P. Huissoon, Robotic laser welding: seam sensor and laser focal frame registration, *Robotica* 20 (3) (2002) 261–268, <https://doi.org/10.1017/S0263574701003988>.
- [3] “Application of vision to laser welding : increase of operating tolerances using beam-oscillation and filler-wire.” [Online]. Available: [http://pubs.aip.org/liacp/proceedings-pdf/ICALEO/1997/C21/7870012/c21\\_1\\_online.pdf](http://pubs.aip.org/liacp/proceedings-pdf/ICALEO/1997/C21/7870012/c21_1_online.pdf).
- [4] Q.S. Liu, S.M. Mahdavian, D. Aswin, S. Ding, Experimental study of temperature and clamping force during Nd:YAG laser butt welding, *Opt. Laser. Technol.* 41 (6) (2009) 794–799, <https://doi.org/10.1016/j.optlastec.2008.12.002>.
- [5] B. Li, B.W. Shiu, and K.J. Lau, “Principle and simulation of fixture configuration design for sheet metal assembly with laser welding. part 1: finite-element modelling and a prediction and correction method,” 2001.
- [6] B. Siciliano, L. Sciacivco, L. Villani, G. Oriolo, *Robotics*, Springer London, London, 2009.
- [7] R. (Robert R. Waiboer and Print Partners Ipskamp), *Dynamic modelling, identification and simulation of industrial robots : for off-line programming of robotised laser welding*. s.n., 2007.
- [8] A. Rout, B.B.V.L. Deepak, B.B. Biswal, Advances in weld seam tracking techniques for robotic welding: a review, *Robot. Comput. Integr. Manuf.* 56 (2019) 12–37, <https://doi.org/10.1016/j.rcim.2018.08.003>.
- [9] J. Muhammad, H. Altun, E. Abo-Serie, Welding seam profiling techniques based on active vision sensing for intelligent robotic welding, *Int. J. Adv. Manuf. Technol.* 88 (1–4) (2017) 127–145, <https://doi.org/10.1007/s00170-016-8707-0>.
- [10] M. de Graaf, R. Aarts, B. Jonker, J. Meijer, Real-time seam tracking for robotic laser welding using trajectory-based control, *Control Eng Pract* 18 (8) (2010) 944–953, <https://doi.org/10.1016/j.conengprac.2010.04.001>.
- [11] H.S. Kang, J. Suh, T.D. Cho, Study on robot application technology for laser welding, in: *ICSMA 2008 - International Conference on Smart Manufacturing Application*, 2008, pp. 354–356, <https://doi.org/10.1109/ICSMA.2008.4505551>.
- [12] A. Pischetsrieder, “Adaptive welding of fillet welds using a fast seam-tracking sensor in combination with a standard industrial robot.” [Online]. Available: <http://proceedings.spiedigitallibrary.org/>.
- [13] W. Zhang, Z. Zheng, X. Ma, Q. Chen, D. Du, Circular sub-window multi-step GPI method in seam tracking of welding robot based on 3D vision. *Lecture Notes in Computer Science (Including subseries Lecture Notes in Artificial Intelligence and Lecture Notes in Bioinformatics)*, 2008, pp. 916–926, [https://doi.org/10.1007/978-3-540-88518-4\\_98](https://doi.org/10.1007/978-3-540-88518-4_98).
- [14] W. Zhang, Q. Chen, G. Zhang, Z. Sun, D. Du, Seam tracking of articulated robot for laser welding based on visual feedback control. *Lecture Notes in Control and Information Sciences*, 2007, pp. 281–287, [https://doi.org/10.1007/978-3-540-73374-4\\_33](https://doi.org/10.1007/978-3-540-73374-4_33).
- [15] X. Gao, D. You, S. Katayama, Seam tracking monitoring based on adaptive Kalman filter embedded elman neural network during high-power fiber laser welding, *IEEE Trans. Ind. Electron.* 59 (11) (2012) 4315–4325, <https://doi.org/10.1109/TIE.2012.2193854>.
- [16] N. Wang, K. Zhong, X. Shi, X. Zhang, A robust weld seam recognition method under heavy noise based on structured-light vision, *Robot. Comput. Integr. Manuf.* 61 (2020) 101821, <https://doi.org/10.1016/j.rcim.2019.101821>.
- [17] M. Nilsen, F. Sikström, A.-K. Christiansson, A. Ancona, Monitoring of varying joint gap width during laser beam welding by a dual vision and spectroscopic sensing system, *Phys. Procedia* 89 (2017) 100–107, <https://doi.org/10.1016/j.phpro.2017.08.014>.
- [18] P.J. Wang, W.J. Shao, S.H. Gong, P.J. Jia, G. Li, High-precision measurement of weld seam based on narrow depth of field lens in laser welding, *Sci. Technol. Weld. Joining* 21 (4) (2016) 267–274, <https://doi.org/10.1080/13621718.2015.1104094>.
- [19] X. Gao, D. You, S. Katayama, Infrared image recognition for seam tracking monitoring during fiber laser welding, *Mechatronics* 22 (4) (2012) 370–380, <https://doi.org/10.1016/j.mechatronics.2011.09.005>.
- [20] B. Xue, B. Chang, G. Peng, Y. Gao, Z. Tian, D. Du, G. Wang, A vision based detection method for narrow butt joints and a robotic seam tracking system, *Sensors* 19 (5) (2019) 1144, <https://doi.org/10.3390/s19051144>.
- [21] Z. Jia, T. Wang, J. He, L. Li, K. Wu, Real-time spatial intersecting seam tracking based on laser vision stereo sensor, *Measurement (Lond)* 149 (2020), <https://doi.org/10.1016/j.measurement.2019.106987>.
- [22] C.H. Kim, T.Y. Choi, J.J. Lee, J. Sun, K.T. Park, H.S. Kang, Development of welding profile sensor and its application, in: *ICSMA 2008 - International Conference on Smart Manufacturing Application*, IEEE Computer Society, 2008, pp. 24–29, <https://doi.org/10.1109/ICSMA.2008.4505606>.
- [23] L. Zhou, T. Lin, S.B. Chen, Autonomous acquisition of seam coordinates for arc welding robot based on visual servoing, *J. Intell. Robot. Syst.* 47 (3) (2006) 239–255, <https://doi.org/10.1007/s10846-006-9078-9>.
- [24] D. Iakovou, R. Aarts, J. Meijer, and B. Jonker, “Perimetric sensor for the detection and following of complex seam trajectories in robotic laser welding paper 1901.” [Online]. Available: [http://pubs.aip.org/liacp/proceedings-pdf/ILSC/2007/1901/7872894/1901\\_1\\_online.pdf](http://pubs.aip.org/liacp/proceedings-pdf/ILSC/2007/1901/7872894/1901_1_online.pdf).
- [25] M. Kos, E. Arko, H. Kosler, M. Jezeršek, Remote-laser welding system with in-line adaptive 3D seam tracking and power control. *Procedia CIRP*, Elsevier B.V., 2019, pp. 1189–1194, <https://doi.org/10.1016/j.procir.2019.03.290>.
- [26] M. Nilsen, F. Sikström, A.-K. Christiansson, Adaptive control of the filler wire rate during laser beam welding of squared butt joints with varying gap width, *Int. J. Adv. Manuf. Technol.* 102 (9–12) (2019) 3667–3676, <https://doi.org/10.1007/s00170-019-03325-w>.
- [27] Z. Luo, J.S. Dai, C. Wang, F. Wang, Y. Tian, M. Zhao, Predictive seam tracking with iteratively learned feedforward compensation for high-precision robotic laser welding, *J. Manuf. Syst.* (2012) 2–7, <https://doi.org/10.1016/j.jmsy.2011.03.005>.
- [28] B. Regaard, S. Kaierle, R. Poprawe, Seam-tracking for high precision laser welding applications—methods, restrictions and enhanced concepts, *J. Laser Appl.* 21 (4) (2009) 183–195, <https://doi.org/10.2351/1.3267476>.
- [29] W. Cieszyński, M. Zięba, J. Reiner, Real time trajectory correction system of optical head in laser welding, *Acta Mechanica et Automatica* 9 (4) (2015) 265–269, <https://doi.org/10.1515/ama-2015-0042>.
- [30] W.J. Shao, Y. Huang, Y. Zhang, A novel weld seam detection method for space weld seam of narrow butt joint in laser welding, *Opt. Laser. Technol.* 99 (2018) 39–51, <https://doi.org/10.1016/j.optlastec.2017.09.037>.
- [31] M. Yan, K. Zhang, D. Liu, H. Yang, Z. Li, Autonomous programming and adaptive filling of lap joint based on three-dimensional welding-seam model by laser scanning, *J. Manuf. Process.* 53 (2020) 396–405, <https://doi.org/10.1016/j.jmapro.2020.03.034>.
- [32] L. Wang, Y. Liu, W. Zhou, Vision algorithm for robot seam tracking based on laser ranging, *Robot. Comput. Integr. Manuf.* 67 (2021) 102026, <https://doi.org/10.1016/j.rcim.2020.102026>.
- [33] J. Li, Y. Zhang, L. Wang, LSPF-Tracker: autonomous laser stripe feature point extraction algorithm for robotic welding seam tracking, *J. Manuf. Syst.* 58 (2021) 36–46, <https://doi.org/10.1016/j.jmsy.2020.11.005>.
- [34] L. Wang, Y. Liu, Image denoising method of seam images with deep learning for laser vision seam tracking, *Opt. Lasers. Eng.* 137 (2021) 106368, <https://doi.org/10.1016/j.optlaseng.2020.106368>.
- [35] Y. Zhang, P. Li, Performance analysis of object detection algorithms for robotic welding applications in a planar environment, *J. Manuf. Syst.* 58 (2021) 287–295, <https://doi.org/10.1016/j.jmsy.2020.12.006>.
- [36] Y. Zhang, B. Wu, A four-step welding seam tracking system for symmetrical robotic welding processes, *J. Manuf. Process.* 64 (2021) 1171–1181, <https://doi.org/10.1016/j.jmapro.2021.04.023>.
- [37] Y. Zhang, P. Li, Multi-layer sensing and intelligent control method of a novel mobile welding robot, *Robot. Comput. Integr. Manuf.* 63 (2020) 101909, <https://doi.org/10.1016/j.rcim.2019.101909>.
- [38] Z. Pan, H. Zhang, B. Wu, Closed-loop robot control for seam-tracking and force control in robotic friction stir welding, *Robot. Comput. Integr. Manuf.* 67 (2021) 102054, <https://doi.org/10.1016/j.rcim.2020.102054>.
- [39] Y. Liu, L. Wang, Novel seam tracking technique with a four-step method for robotic welding, *J. Manuf. Process.* 56 (2020) 1229–1239, <https://doi.org/10.1016/j.jmapro.2020.06.049>.
- [40] Y. Yamazaki, Y. Abe, Y. Hioki, M. Nakatani, A. Kitagawa, K. Nakata, Fundamental study of narrow-gap welding with oscillation laser beam, *Weld. Int.* 30 (9) (2016) 699–707, <https://doi.org/10.1080/09507116.2016.1142193>.
- [41] A. Müller, S.F. Goecke, M. Rethmeier, Laser beam oscillation welding for automotive applications, *Weld. World* 62 (5) (2018) 1039–1047, <https://doi.org/10.1007/s40194-018-0625-3>.
- [42] R.P. Martukanitz, I. Stol, J.F. Tressler, and C.J. Warren, “Development of the laser stir welding process for aluminum laser beam welding.” [Online]. Available: [http://pubs.aip.org/liacp/proceedings-pdf/ICALEO/2005/1208/7872521/1208\\_1\\_online.pdf](http://pubs.aip.org/liacp/proceedings-pdf/ICALEO/2005/1208/7872521/1208_1_online.pdf).
- [43] G. Göbel, B. Brenner, and E. Beyer, “NEW Application possibilities for fiber laser welding.” [Online]. Available: [http://pubs.aip.org/liacp/proceedings-pdf/ILSC/2007/209/7874528/209\\_1\\_online.pdf](http://pubs.aip.org/liacp/proceedings-pdf/ILSC/2007/209/7874528/209_1_online.pdf).
- [44] D.M. Boldrin, M. Colopi, S. D’arcangelo, L. Caprio, A. Gökhan Demir, and B. Previtali, “High speed videography of gap bridging with beam oscillation and wire feeding during the laser welding of stainless steel and aluminum alloys”.
- [45] J. Li, et al., Analysis and improvement of laser wire filling welding process stability with beam wobble, *Opt. Laser. Technol.* 134 (2021), <https://doi.org/10.1016/j.optlastec.2020.106594>.
- [46] K. Rubben1, H. Mohrbacher1, and E. Leirman2, “Advantages of using an oscillating laser beam for the production of tailored blanks.” [Online]. Available: <http://proceedings.spiedigitallibrary.org/>.
- [47] M.P. Vänskä, V. Kujanpää, E.M. Westin, and T. Torvinen, “Short focal length scanner fiber laser welding of stainless steel sheets and tubular products.” [Online]. Available: [http://pubs.aip.org/liacp/proceedings-pdf/ILSC/2009/766/7877784/766\\_1\\_online.pdf](http://pubs.aip.org/liacp/proceedings-pdf/ILSC/2009/766/7877784/766_1_online.pdf).
- [48] M. Köhler, T. Tóth, A. Kreybohm, J. Hensel, K. Dilger, Effects of reduced ambient pressure and beam oscillation on gap bridging ability during solid-state laser beamwelding, *J. Manuf. Mater. Process.* 4 (2) (2020), <https://doi.org/10.3390/jmmp4020040>.
- [49] A. Müller, S.F. Goecke, M. Rethmeier, Laser beam oscillation for fillet welding, *Weld. World* 58 (6) (2014) 865–872, <https://doi.org/10.1007/s40194-014-0165-4>.
- [50] A. Müller, S.F. Goecke, P. Sievi, F. Albert, M. Rethmeier, Laser beam oscillation strategies for fillet welds in lap joints. *Physics Procedia*, Elsevier B.V., 2014, pp. 458–466, <https://doi.org/10.1016/j.phpro.2014.08.149>.
- [51] P. Fixemer, F. Albert, P. Sievi, T. Graham, Seam guided laser remote welding with automated gap bridging, *Laser Technik J.* 12 (2) (2015) 38–41, <https://doi.org/10.1002/latj.201500012>.
- [52] M.J. Reiter, J. Cho, D.F. Farson, and M. Mehl, “Analysis and control of penetration depth fluctuations in single-mode fiber laser welds.” [Online]. Available: [http://pubs.aip.org/liacp/proceedings-pdf/ILSC/2009/800/7878159/800\\_1\\_online.pdf](http://pubs.aip.org/liacp/proceedings-pdf/ILSC/2009/800/7878159/800_1_online.pdf).



- [53] C. Thiel, A. Hess, R. Weber, T. Graf, Stabilization of laser welding processes by means of beam oscillation. *Laser Sources and Applications*, SPIE, 2012, p. 84330V, <https://doi.org/10.1117/12.922403>.
- [54] J. Canny, A computational approach to edge detection, *IEEE Trans. Pattern. Anal. Mach. Intell. PAMI-8* (6) (1986) 679–698, <https://doi.org/10.1109/TPAMI.1986.4767851>.
- [55] G. Bradski, *The OpenCV Library*, Dr. Dobb's J. Softw. Tools (2000).
- [56] P.V. Hough, *Methods and means for recognising complex patterns*. 1962.
- [57] ABB Robotics. *Application manual - controller software IRC5*, 2014.
- [58] ABB Robotics. *Operating manual - IRC5 integrators guide*, 2019.
- [59] Y. Liu, A.W. Hoover, I.D. Walker, A timing model for vision-based control of industrial robot manipulators, *IEEE Trans. Robotics* 20 (5) (2004) 891–898, <https://doi.org/10.1109/TRO.2004.829460>.
- [60] International Organization for Standardization, “Welding and allied processes – classification of geometric imperfections in metallic materials – Part 1: fusion welding.” Geneva, CH, 2007.